JOURNAL OF APPLIED ELECTROCHEMISTRY 15 (1985) 399–404

Impedance of the sintered nickel positive electrode

R. T. BARTON, M. HUGHES, S. A. G. R. KARUNATHILAKA, N. A. HAMPSON

Department of Chemistry, University of Technology, Loughborough, Leicestershire, LE11 3TU, UK

Received 18 June 1984; revised 25 July 1984

Impedance measurements have been made on a mini electrode disposed between two large (identical) counter electrodes. A general mechanism is obtained for the electrode behaviour from the experimental data. The electrode reaction is two step and complex. Where comparison is possible agreement is obtained with earlier work.

1. Introduction

Interest in the behaviour of the nickel oxide electrode, which has been reviewed by Milner and Thomas [1] and Briggs [2] stems from its popular use in nickel–iron, nickel–cadmium and nickel–zinc cells. These cells possess high energy densities, are capable of high rate applications and have excellent recycling characteristics. The nickel–cadmium cell for example is most frequently used for aircraft applications.

The nickel oxide electrode is of the plaque type manufactured by sintering fine-grain nickel particles on to a nickel grid which acts as a mechanical support and current collector thus assuring low electronic resistance to the highly dispersed active materials. The resulting plaque has a porosity of about 80%. The porous structure of the sinter readily permits access of the electrolyte, thus maintaining a low resistance.

The plaque is impregnated (under vacuum) with nickel nitrate, which is then converted to nickel hydroxide by immersion in hot alkali and then oxidized to the nickel oxyhydroxide [3].

The existance of several possible oxidation states of the nickel in the hydrated oxides has complicated the establishment of the fundamental kinetics of the nickel oxide electrode.

The recycling process at the solid–liquid interface is usually represented as the following:

$$Ni(OH)_2 + OH^- \underset{\text{discharge}}{\overset{\text{charge}}{\rightleftharpoons}} NiO{\cdot}OH + H_2O + e \quad (1)$$

The charge is propagated in the solid phase by a proton transfer mechanism. It is assumed that the process is diffusion of protons either by means of hydrogen bonds in the oxyhydroxide or along intercalated water layers in the crystal lattice or both. The charging process is accompanied by the formation of a hydrogen-bonded structure possessing a higher degree of crystal symmetry than found in the discharged state. During discharge, these hydrogen bonds are continuously broken and the structure transforms back to a free hydroxyl configuration [4].

This reaction is however complicated by oxygen evolution and by the fact that the states of oxidation are not stoichiometric. There are at least two modifications of both the charged material β-NiOOH and γ-NiOOH and of the discharged material α-$Ni(OH)_2$ and β-$Ni(OH)_2$. The β-phases of both the charged and discharged states are normally predominant under standard conditions.

The reduced α form has the formula $3Ni(OH)_2 \cdot 2H_2O$ and is unstable on standing on open circuit or cycling [5]. The more stable β-$Ni(OH)_2$ has the Brucite structure. Kober [4] has shown the discharged states to have a hexagonal layer structure isomorphic with the space group D_{3d}^3. The β-$Ni(OH)_2$ consists of NiO_2 planes separated by nonhydrogen-bonded hydroxyl groups. The separation is greater in α-$Ni(OH)_2$; the intervening space is presumed to be occupied by unordered water molecules. This separation decreases in the oxidized forms.

Micka and Roušar [6] suggest that the composition of the oxidized form is intermediate between $NiO_{1.5}$ and $NiO_{1.8}$, the upper limit of the oxidized state being dependant on various conditions. The abundance of γ-NiOOH can be enhanced by a

0021-891X/85 $0.300 + .12

higher charging rate, the amount of electricity charged and high electrolyte concentrations [7–9]. The average oxidation number of nickel is assumed to be 3.67.

The electrode reactions are therefore likely to involve the adsorption of the hydroxyl ion and subsequent charge transfer at a porous surface.

This paper describes experiments in which small (mini) electrodes were investigated in the form of two terminal cells.

2. Experimental procedure

An electrode holder was initially constructed from perspex. The walls and base of the holder were slotted with a spacing of 5 mm to accommodate individual electrode plates. A 1 cm^2 electrode was cut to size and disposed between two complete electrode plates, this arrangement allowing impedance measurement of the mini 1 cm^2 electrode only. The two large area electrodes (13 cm x 7 cm) were connected in parallel and formed the counter electrode and were assumed to contribute negligible impedance to the cell. The electrolyte was the conventional one for the nickel–cadmium cell (i.e. 5 M.)

The electrodes were charged at constant current until the over-voltage was in excess of 1.6 V, and discharges were carried out at the 4C rate to a final cell e.m.f. of 1 V. [10].

The impedance measuring technique for which a Solatron 1170 frequency response analyser coupled to a Kemitron PS40 potentiostat, has been described earlier [11]. The voltage was measured across the cell and the current measured across a non-inductive 26 mΩ resistor. This arrangement was preferred since it ensured the elimination of any voltage drop across long leads. The cell was connected to the potentiostat in the two terminal mode.

The electrodes were allowed to rest for one hour after charging or discharging prior to an impedance run. Impedance data were collected on punched paper tape and transferred to the Honeywell Multics computer for subsequent analysis.

3. Results and discussion

Fig. 1 shows the complex plane impedance over the frequency range 10 kHz to 10 mHz for a 0% state-of-charge nickel electrode. At high frequencies a flattened semi-circle can be seen which relaxes to a further shape which subtends an angle of 43° at lower frequencies. Fig. 2 shows the impedance plot of a nickel electrode at 100% state-of-charge. There is a significant reduction in the magnitude of the semi-circle, the dihedral has an angle of about 35° down to 100 mHz, this angle increasing to 50° at the lower frequencies.

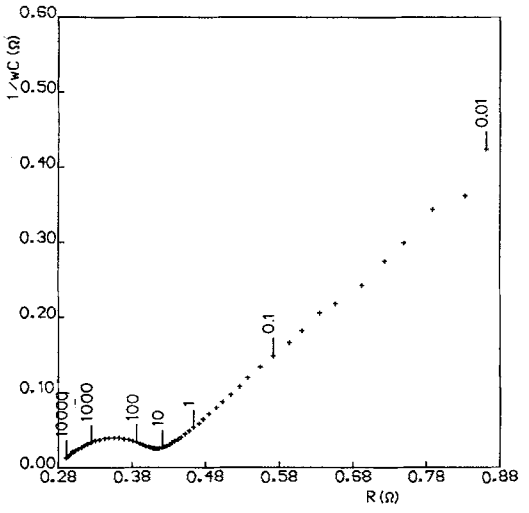

Fig. 1. Slüyters plot of a 0% state-of-charge nickel electrode (frequency in Hz).

The Slüyters plots for the complete range of states-of-charge reveal a rapid decrease in the magnitude of the flattened semi-circle from 0% to 100%.

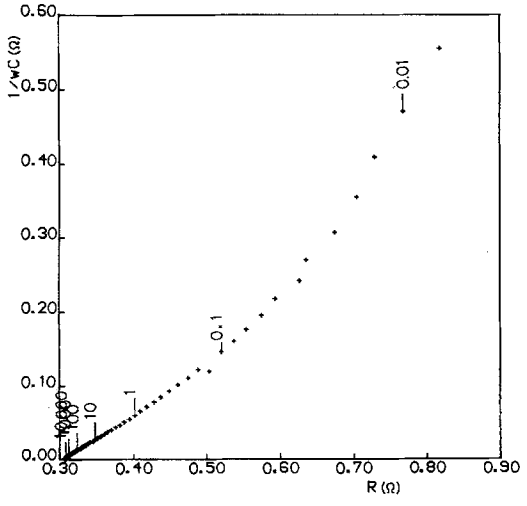

Fig. 2. Slüyters plot of a 100% state-of-charge nickel electrode, (frequency in Hz).

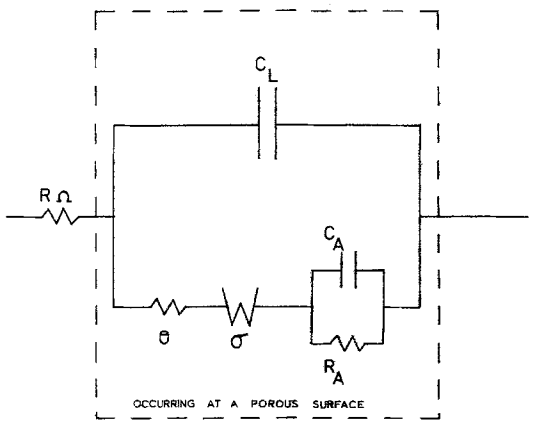

Fig. 3. The cell analogue.

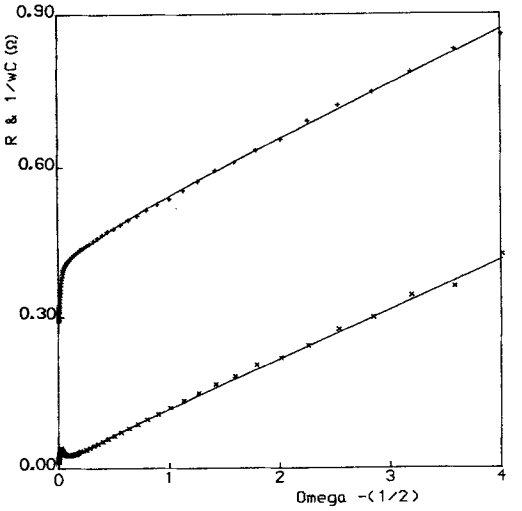

Fig. 4. Randles plot of the experimental data and the best fit obtained for a 0% state-of-charge electrode.

If we follow the reported mechanisms for the nickel electrode the simplest process for the overall exchange reaction between Ni(II) and Ni(III) can best be represented as:

$$NiO + OH^- \rightleftharpoons NiOOH^-_{ads} \quad (2)$$

$$NiOOH^-_{ads} \longrightarrow NiOOH + e^- \quad (3)$$

where the hydroxide ion is adsorbed and undergoes subsequent reaction with the NiO to form the Ni(III) state.

The analogue used to describe this electrochemistry is shown in Fig. 3. Where R_Ω is the solution resistance, θ the charge transfer resistance, σ the Warburg slope, C_L the double layer capacitance, C_A the capacitance and R_A the resistance characteristic of the process (2) which preceeds the charge transfer. The battery manufacturer seeks to optimize the energy output of the present electrodes and consequently it has become customary to increase the effective surface area by arranging for the electrode to be porous. This disposition of the electrode in three dimensions introduces complications into the analogue representation of the electrode behaviour vis-a-vis the planar one. De Levie [12] has shown that for infinitely long pores the planar electrode behaviour in the complex plane may be 'transformed' into that corresponding to the porous one by square rooting the modulus of the impedance and halving the argument. This halving factor can readily be introduced into our model via the computer; however, a better test is obtained by isolating a general factor γ which is

Table 1. Values of the computed circuit components

Charge (%)	$R\Omega$ (Ohms)	*Theta* (Ohms)	C_L (Farads)	*Sigma* ($s^{-\frac{1}{2}}$)	C_A (Farads)
100	0.31	2.02E–5	3.86	2.54E–2	57.31
90	0.36	3.70E–5	3.13	2.32E–2	66.66
80	0.36	3.52E–5	4.83	3.59E–2	32.42
70	0.34	3.21E–5	0.29	3.07E–2	28.99
60	0.33	3.07E–5	5.41	3.53E–2	39.53
50	0.33	5.84E–5	4.46	4.32E–2	41.28
40	0.31	4.01E–4	4.86	4.40E–2	51.18
30	0.31	1.92E–4	5.46	2.64E–2	73.65
20	0.35	5.39E–4	6.37	2.26E–2	121.03
10	0.32	4.38E–4	0.25	2.75E–2	68.91
0	0.29	1.36E–2	6.2E–2	4.10E–2	48.50

The values of γ and R_A are consistently 0.5 and 1 MΩ respectively.

the power to which the complex impedence has to be raised to generate the observed behaviour from that of an equivalent planar one ($\gamma = 1$ represents a planar electrode, $\gamma = 0.5$ represents an infinitely porous electrode). The computer program used to subsequently process the impedance data sought the best value of γ to fit the data using the process model represented by Equations 2 and 3. It was convincing proof of the correctness of this reasoning that γ turned out to be 0.5 at every state-of-charge.

The values of the impedance components were calculated from their approximate values using Taylors theorem neglecting second and higher order terms; a least squares process was then used to reduce the number of equations to that required to solve for each of the circuit elements. The process was repeated a sufficient number of times until accurate values for each of the circuit elements were obtained. The results of the analysis are shown in Table 1.

Fig. 4 shows a Randles plot of the experimental data and the best fit obtained for a 0% state-of-charge electrode. Figs. 5–8 show similar data and corresponding fits on Randles plots for 30%, 60%, 80% and 100% states-of-charge respectively. Fig. 9 shows the best fit on a Slüyters plot for a 0% state-of-charge electrode.

The potential dependance of the planar equivalent θ was determined for the nickel electrode by stepping cathodically and re-determining the impedance. A plot of log θ versus e.m.f. was linear with a slope of 36 mV per decade; this is shown in Fig. 10.

For a simple single electron transfer the Tafel slope should be 120 mV. The electrode process must be represented by a scheme of the form of Equations 2 and 3. This follows from the excellent agreement between the experimental data and the calculated response which together with the consistancy of the γ value of 0.5 over seven decades of frequency makes any other scheme very unlikely. However, the precise identity of the Equations 2

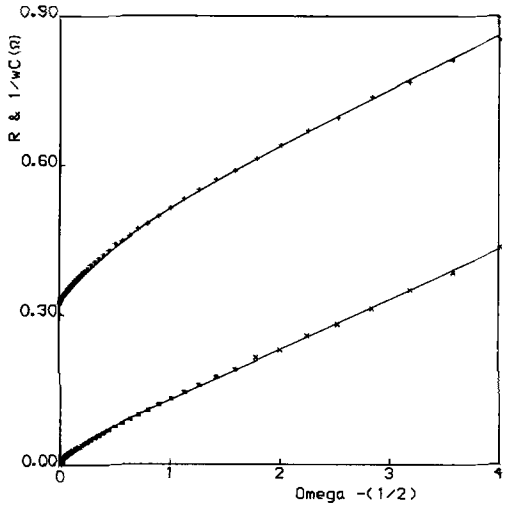

Fig. 6. As for Fig. 4. but for a 60% state-of-charge electrode.

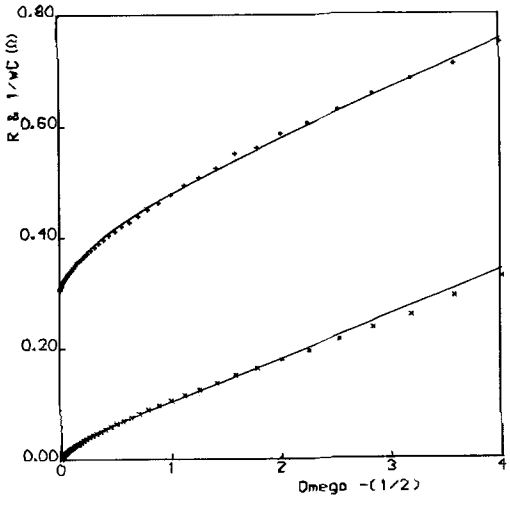

Fig. 5. As for Fig. 4. but for a 30% state-of-charge electrode.

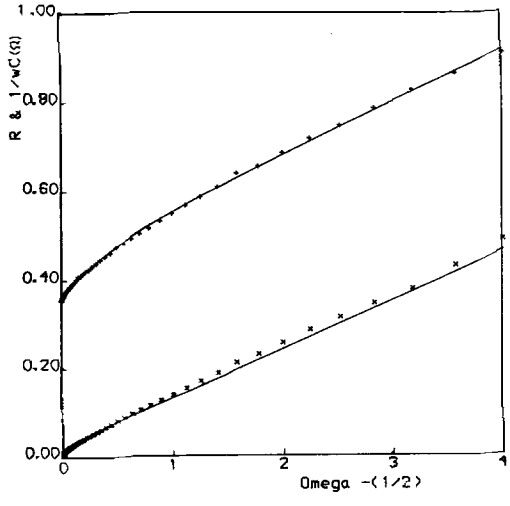

Fig. 7. As for Fig. 4. but for a 80% state-of-charge electrode.

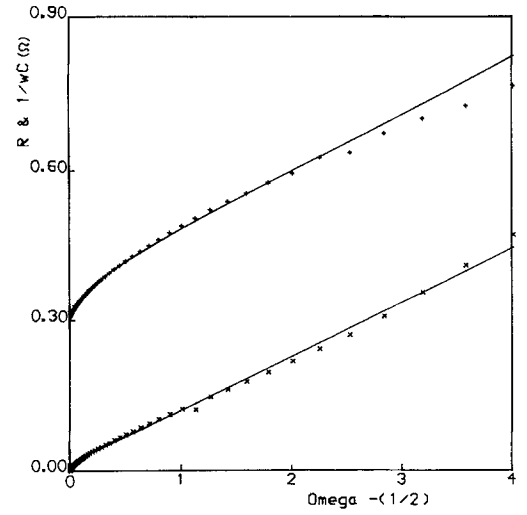

Fig. 8. As for Fig. 4. but for a 100% state-of-charge electrode.

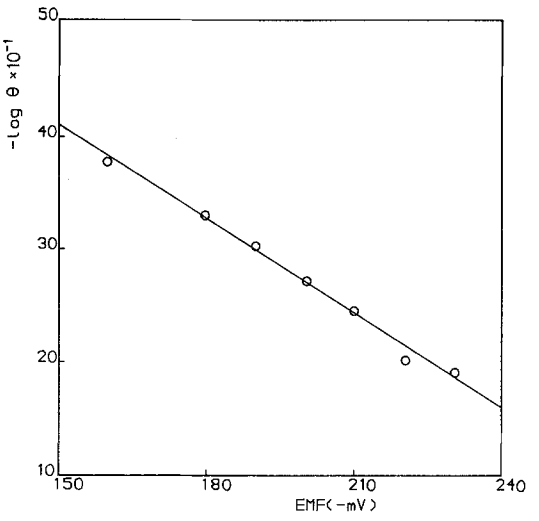

Fig. 10. Tafel plot of log θ versus e.m.f.

and 3 cannot be determined with absolute certainty. The value of $d\ln\theta/dE$ is a Tafel slope and if the Equations 2 and 3 are taken prima facie then the slope would be expected to be 120 mV. The value of 36 mV suggests a reaction involving three electrons. A survey of the literature indicates that Tafel data comparative to the present study are scarce. Russian workers [13] have reported that in the high current region of the cathodic Tafel region b was approximately 40 mV and about 120 mV in the low current region. The value of b varied also with the number of cycles taken in the linear sweep voltammetry experiment. It is rather difficult to compare our results with these. Examination of the literature in order to find a mechanism which implies a 40 mV slope is also unrewarding since the mechanism of the industrial hydrated nickel hydroxide electrode is a matter of considerable controversy [5]. MacArthur suggests at one extreme that the overall reaction for α-nickel hydroxide involved a formal six electron change whilst at the other Barnard and co-workers [14] emphasize the importance of the precise nature of the co-existing phases. It seems in the face of this that Tafel data may have limited significance, however, the uniqueness of the straight line of Fig. 10 and correlation coefficient of 0.994 indicates that this may not be completely so. What is important in the present work is that the porous nature of the electrode has been completely allowed for; previous kinetic investigations have not done so and thereby uncertainty may arise from the over-simplifications introduced.

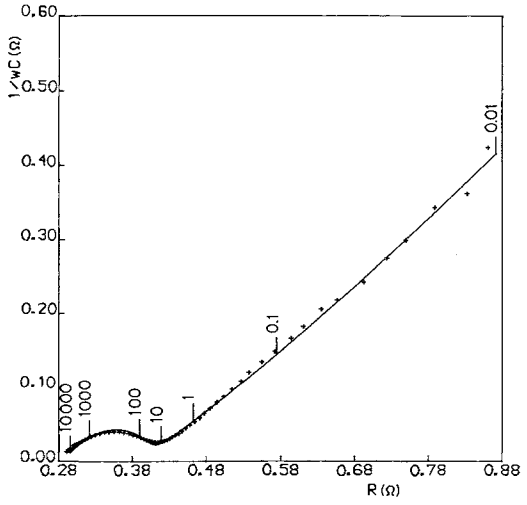

Fig. 9. Slüyters plot of a 0% state-of-charge nickel electrode and the best fit obtained, (frequency in Hz).

It is also of interest to note that throughout the frequency domain and at each state-of-charge γ was always 0.5 and the value of R_A was significant. This indicates that adsorption (Equation 3) may assume a rate determining rôle when the frequency is sufficiently low. The possibility, however, of diffusion within the pore engendering the relaxation represented by R_A and C_A as the frequency is ranged is precluded by this consistency of the R_A and C_A circuit components and the accurate representation of the porous structure (by $\gamma = 0.5$ exactly) through all the experiments.

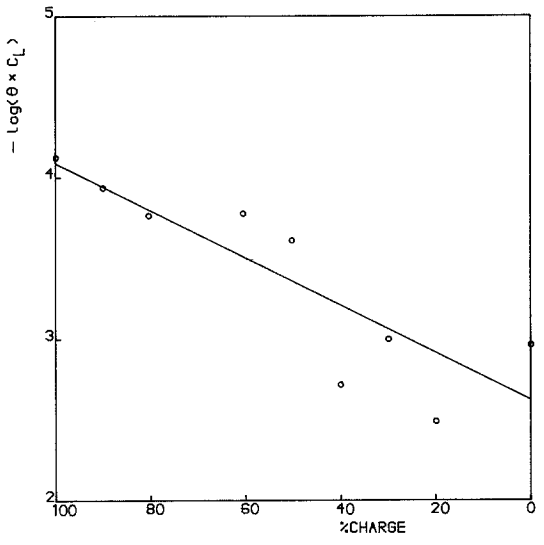

Fig. 11. Plot of log ($C_L\theta$) versus % charge.

The technological target of this work has been the identification of a parameter on which to have a suitable state of charge for the nickel–cadmium cell. An interesting feature to emerge from the work is a correlation between the charge transfer resistance θ corrected for the area by plotting log θC_L versus $\%C$, where C is the state-of-charge (Fig. 11). This shows a general trend of the θC_L product in a downward direction. At this point it is not possible to say whether or not this single electrode parameter can be made to yield the desired information about the whole cell but work is continuing.

Acknowledgements

The authors wish to thank the Procurement Executive, Ministry of Defence, for supporting this work. They would also like to thank Dr J. Knight for his useful comments and criticisms.

References

[1] P. C. Milner and U. B. Thomas, in 'Advances in Electrochemistry and Electrochemical Engineering' Vol. 5, Interscience, New York (1967) 59.
[2] G. W. D. Briggs, Chemical Society Specialist Periodical Reports, Electrochemistry **4** (1974).
[3] E. Hausler in 'Power Sources', Vol. 1, 1966 Research and Development in Non-Mechanical Electrical Power Sources, Edited by D. H. Collins, (1967) p. 287.
[4] F. P. Kober, *J. Electrochem. Soc.* **112** (1965) 1064.
[5] D. M. MacArthur, *ibid.* **117** (1970) 422.
[6] K. Micka and I. Roušar, *Electrochim. Acta* **25** (1980) 1085.
[7] J. P. Harviel, B. Morignat, J. Labat and J. F. Laurent, in 'Power Sources', Vol. 1, 1966 Research and Development in Non-Mechanical Electrical Power Sources, Edited by D. H. Collins, (1967) p. 239.
[8] N. Yu. Uflyand, A. M. Novakovskii and S. A. Rozentsveig *Soviet Electrochem.* **3** (1967) 470.
[9] G. W. D. Briggs and P. R. Snodin, *Electrochim. Acta* **27** (1982) 565.
[10] B. S. Aerospace Series 2G–205: 1976.
[11] N. A. Hampson and M. J. Willars, *Surface Technol.* 7 (1978) 247.
[12] R. de Levie, in 'Advances in Electrochimstry and Electrochemical Engineering' Vol. 6, Interscience New York (1967).
[13] O. G. Malandin, P. D. Lukovtsev and T. S. Tikhonova, *Soviet Electrochem.* 7 (1971) 633.
[14] R. Barnard and C. F. Randell, *J. Power Sources* **9** (1983) 185.